Dryness controls temperature-optimized gross primary productivity across vegetation types

Bingxue Wang [a,1], Weinan Chen [a,b,1], Junhu Dai [b,c,d], Zhaolei Li [a], Zheng Fu [e], Sangeeta Sarmah [a], Yiqi Luo [f], Shuli Niu [a,b,*]

[a] *Key Laboratory of Ecosystem Network Observation and Modeling, Institute of Geographic Sciences and Natural Resources Research, CAS, Beijing 100101, China*
[b] *College of Resources and Environment, University of Chinese Academy of Sciences, Beijing 100049, China*
[c] *Key Laboratory of Land Surface Pattern and Simulation, Institute of Geographic Sciences and Natural Resources Research, CAS, Beijing 100101, China*
[d] *China-Pakistan Joint Research Center on Earth Sciences, CAS-HEC, Islamabad 45320, Pakistan*
[e] *Laboratoire des Sciences du Climat et de l'Environnement, LSCE/IPSL, CEA-CNRS-UVSQ, Université Paris-Saclay, Gif-sur-Yvette 91191, France*
[f] *Center for Ecosystem Science and Society and the Department of Biological Sciences, Northern Arizona University, Flagstaff, AZ 86011, USA*

ARTICLE INFO

ABSTRACT

Temperature response of gross primary productivity (GPP) is a well-known property of ecosystem, but GPP at the optimum temperature (GPP_T_{opt}) has not been fully discussed. Our understanding of how GPP_T_{opt} responds to warming and water availability is highly limited. In this study, we analyzed data at 326 globally distributed eddy covariance sites (79°N-37°S), to identify controlling factors of GPP_T_{opt}. Although GPP_T_{opt} was significantly influenced by soil moisture, global solar radiation, mean annual temperature, and vapor pressure deficit in a non-linear pattern ($R^2 = 0.47$), the direction and magnitude of these climate variables' effects on GPP_T_{opt} depend on the dryness index (DI), a ratio of potential evapotranspiration to precipitation. The spatial pattern showed that soil moisture did not affect GPP_T_{opt} across energy-limited sites with DI < 1 while dominated GPP_T_{opt} across water-limited sites with DI >1. The temporal pattern showed that GPP_T_{opt} was lowered by warming or low precipitation in water-limited sites while energy-limited sites tended to maintain a stable GPP_T_{opt} regardless of changes in air temperature. Vegetation types in humid climates tended to have higher GPP_T_{opt} and were more likely to benefit from a warmer climate since it was not restricted by water conditions. This study highlights that the response of GPP_T_{opt} to global warming depends on the dryness conditions, which explains the nonlinear control of water and temperature over GPP_T_{opt}. Our finding is essential to realistic prediction of terrestrial carbon uptake under future climate and vegetation conditions.

1. Introduction

Gross primary productivity (GPP) is the most important component of the terrestrial carbon cycle and its great variability can lead to large uncertainty in modeled dynamics of terrestrial carbon sequestration (Beer et al., 2010; Friedlingstein et al., 2020). Global warming profoundly affects GPP. Theoretically, ecosystem GPP increases with ambient temperature till the temperature reaches an optimum temperature (T_{opt}) corresponding with peaked GPP (GPP_T_{opt}), above which GPP declines sharply (Huang et al., 2019; Kumarathunge et al., 2019). T_{opt} and GPP_T_{opt} are the two most critical parameters in the temperature response of GPP. Thus, the adjustment of the two key properties to a warmer climate determines the magnitude of future carbon uptake (Way and Yamori, 2014). However, most previous studies on thermal acclimation and adaptation of ecosystem-scale photosynthesis focused on T_{opt} (Kumarathunge et al., 2019; Sendall et al., 2015), less on GPP_T_{opt}. It has been well documented that the inter-annual variability of GPP is determined by peak GPP more than any other drivers (Musavi et al., 2017; Xia et al., 2015; Zhou et al., 2016). Therefore, revealing the key climate variables of maximum photosynthetic capacities contributes to more accurate prediction of GPP and the carbon cycle-climate feedbacks (Gu et al., 2009; Yi et al., 2012).

A recent leaf-level study claimed that the maximum photosynthetic capacity, represented by the maximum rates of Rubisco carboxylation (V_{cmax}), is optimized to the climate variables including light, temperature, vapor pressure and atmosphere pressure across the globe (Smith et al., 2019). Since the mechanisms and parameters of the photosynthesis-temperature response differs between different biological hierarchical levels, knowledge of leaf-level photosynthetic capacity is not necessarily applicable for understanding the controlling factors of GPP and its peak rate (GPP_T_{opt}) at the ecosystem scale (Huang et al., 2019; Smith et al., 2019). Although Huang et al. investigated the determinant of the temporal variation in GPP_T_{opt} globally (Huang et al., 2018), the major climate variables of the spatial variation of GPP_T_{opt} is still unknown.

Warming stimulates leaf-level photosynthesis at high soil moisture but reduces it under dry spells (Humphrey et al., 2018; Reich et al., 2018; Smith and Dukes, 2018), thus it is reasonable to hypothesize that water availability also influences the response of GPP_T_{opt} to temperature. Previous studies have found that the inter-annual variation of terrestrial carbon uptake and atmospheric CO_2 growth rate is strongly correlated to the terrestrial water storage, indicating a close interplay between carbon and hydrological cycles (Humphrey et al., 2018). However, it is still unknown how the responses of GPP_T_{opt} to different climate variables varied with dryness conditions.

Carbon and water cycles in the terrestrial ecosystems are closely coupled. It is well-described by Budyco's curve through incorporating the concept of water and energy limits that evapotranspiration was mainly controlled by the balance between potential evapotranspiration and precipitation (i.e. the dryness index, DI) (Budyko et al., 1974; Potter and Zhang, 2009; Yi and Jackson, 2021) (Fig. 1). When DI < 1, evapotranspiration is limited by available energy; when DI > 1, evapotranspiration is limited by available water (Fig. 1). Given the close relationship between GPP and evapotranspiration (Beer et al., 2009; Yu et al., 2008), the concept of water and energy limits possibly applies to the determinant climate variables of GPP_T_{opt} as well. Additionally, different vegetation types vary in climatic preference (Lin et al., 2015; Wang et al., 2017; Whittaker, 1975). Cropland, grassland and forest naturally differ in V_{cmax} and peak vegetation growth (Huang et al., 2018). None has ever studied the variation of GPP_T_{opt} among vegetation types and teases apart the effects of vegetation types and different climate variables.

Using data from 326 FLUXNET eddy covariance sites across large geographical gradients from 37°S to 79°N, we explore the major climate variables of GPP_T_{opt} across space. Extensive ecological researches have
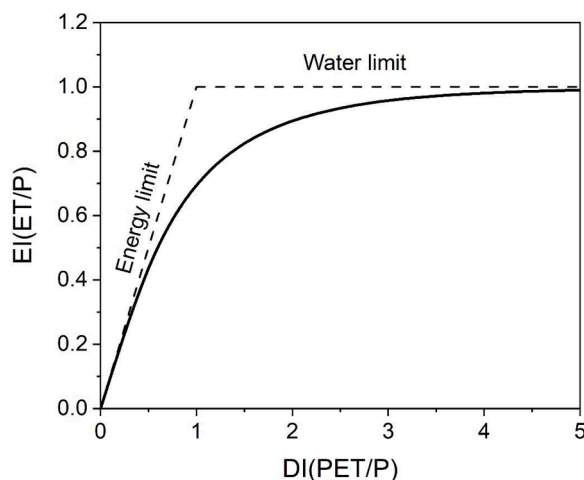
demonstrated that control of water over carbon process is nonlinear (Huxman et al., 2004; Luo et al., 2017) across large geographic areas while within a site carbon processes usually respond linearly to available water (Luo et al., 2017). We hypothesize that GPP_T_{opt} responds to water availability and other environmental drivers non-linearly across the 326 sites (H1). The response of GPP_T_{opt} to different climate variables depends on dryness conditions, i.e., water availability determines GPP_T_{opt} in water-limited ecosystems while temperature boosts GPP_T_{opt} in energy-limited ecosystems (H2). We also hypothesize that GPP_T_{opt} respond to climate variables differently among vegetation types (H3).

2. Material and methods

2.1. Site information and climate data

We obtained daily mean GPP and air temperature from standardized files of the LaThuile and FLUXNET2015 databases. The data were quality-controlled and gap-filled by consistent methods as described in previous reports (Chu et al., 2017; Niu et al., 2012). Data with remained gaps less than 5% in a whole year were selected for further analysis, leaving a total of 326 sites with 1634 site-years data spanning from 37°S to 79°N (Fig. S1). Daily mean GPP and air temperature (T_{air}) instead of hourly data was used to generate GPP-T_{air} response curve, avoiding the influence from the diurnal pattern. Specifically, for each site-year, the daily air temperatures were binned in 1 °C. The daily air temperature and the corresponding GPP in each temperature bin was averaged to construct the GPP-T_{air} response curve. The peaked GPP (GPP_T_{opt}) was determined by calculating the running mean of every three temperature bins.

Mean annual temperature (MAT, °C), mean annual precipitation (MAP, mm yr^{-1}), growing season temperature (GST, °C), growing season precipitation (GSP, mm yr-1), global solar radiation (GSR, MJ m^{-2} d^{-1}) and growing season vapor pressure deficit (VPD, kPa) of each site were obtained from World Clim (Fick and Hijmans, 2017), which are the average for the years 1970–2000. The warmest quarter in a year is considered as the growing season. Humidity index was obtained from FAO dataset (Food and Agriculture Organization of the United Nations, 2015), which is calculated the ratio of precipitation to potential evapotranspiration (P/PET). The reciprocal of humidity index is dryness index (DI, PET/P). Soil moisture (mm) is obtained from CPC soil moisture data provided by the NOAA/OAR/ESRL PSD, Boulder, Colorado, USA, from their Web site at https://www.esrl.noaa.gov/psd/. These data were used to investigate the spatial variation in GPP_T_{opt}.

Vegetative patterns of the sites used in this study were divided into 13 vegetation types according to the International Geosphere-Biosphere Programme (IGBP) (Peel et al., 2007): deciduous broadleaf forest (DBF, $n = 42$), evergreen broadleaf forest (EBF, $n = 26$), evergreen needle leaf forest (ENF, $n = 77$), deciduous needle-leaf forest (DNF, $n = 1$), mixed forest (MF), closed shrubland (CSH), opened shrubland (OSH), grassland (GRA, $n = 61$), cropland (CRO, $n = 34$), savannah (SAV, $n = 12$), woody savannah (WSA, $n = 6$), and wetland (WET, $n = 32$). For the statistical analysis, closed shrubland (CSH, $n = 8$), opened shrubland (OSH, $n = 14$) are merged to shrubland (SH). Savannah (SAV) and woody savannah (WSA) were merged into savannah (SAV). The global vegetation distribution was derived from MODIS (MOD12Q1 Land Cover Science Data Product) at a spatial resolution of 1 km using the classification scheme of IGBP.

2.2. Statistical analysis

GPP_T_{opt} of each site was averaged across multiple years of data. The response of GPP_T_{opt} to climate variables was examined by ridge regression in order to control the collinearity of climate variables across space. GPP_T_{opt} was logarithm transformed to meet the assumption of homogeneity of variance. We further estimated the relative contributions of climate variables by traditional R square partitioning of

Fig. 1. A Budyko curve (revised from Yi and Jackson, 2021). When PET < P, evapotranspiration is limited by available energy; when PET > P, evapotranspiration is limited by available water. Here, EI = ET/P, DI = PET/P, where ET is evapotranspiration, PET is potential evapotranspiration, *P* is precipitation.

multivariate regression and gradient boost regression (machine learning) using "hier.part" and "gbm" packages, respectively.

The relationship between each climate variable and GPP_T_{opt} was examined by polynomial regression and localized polynomial regression (LOESS). We found that GPP_T_{opt}-water availability response function is nonlinear saturating and GPP_T_{opt}-energy response function is concave down. We estimated the saturation point of water availability and turning points of energy using breaking point analysis with R package "segmented".

We analyzed the interaction between climate variables and DI as well as vegetation types by analysis of variances (ANOVA). Rolling window analysis was applied to climate variables to investigate the effects of DI on the partial slope of GPP_T_{opt} to climate variables with window size of 90 sites. We first sorted the 326 sites by DI. Then the mean DI was calculated for every neighboring 90 sites and a multivariate regression was performed within each group with GPP_T_{opt} as response variable and SM, VPD, MAT and GSR as explanatory variables. By testing with different sites of moving window, the 90 sites moving-window allowed a sufficient sample size and most robust goodness of fit for the regression analysis although the results were similar among different sites of moving windows. Based on previous analysis that groups the 326 sites by DI, within each DI group, the function between climate variables and GPP_T_{opt} is linear except for GSR. Thus we used the following function in each 90 neighboring sites.

GPP_T_{opt}= f(SM, VPD, MAT, GSR, GSR^2, GSR^3)

The responses of GPP_T_{opt} to each climate variable were considered as the effect of each climate variable with other climate variables controlled. Then we plotted the partial coefficients derived from this function against the average DI of the corresponding sites. R package "zoo" was used to perform the rolling window analysis.

Then we tested the effects of vegetation types on GPP_T_{opt} using the function below:

GPP_T_{opt}= f((SM, SM^2, VPD, MAT, GSR, GSR^2, GSR^3)*vegetation types)

This function was then used to predict the global distribution of current GPP_T_{opt}.

The average MAT, SM, VPD, GSR and DI are calculated for each vegetation type to evaluate the climate preference (Yi and Jackson, 2021). The sensitivities of GPP_T_{opt} to SM (SM$_{sen}$) and MAT (MAT$_{sen}$) were estimated for each vegetation types. The normalized GPP_T_{opt} of each vegetation type is calculated by setting climate variables at the average level (SM=345mm, VPD=0.78 kPa, MAT=9.6 °C, GSR=13.4 MJ m^{-2} d^{-1}). Principle component analysis (PCA) was used to investigate the relation between climate preference and the sensitivity of GPP_T_{opt} to climate variables as well as normalized GPP_T_{opt} among vegetation types.

The temporal variation of GPP_T_{opt} in response to MAT and MAP was investigated using linear mixed-effect model with R package "nlme". Site was treated as random effect, allowing both slope and intercept of regression to vary between sites. Sites that have more than five years' data were used in the analysis (Fig. S2). We divided sites into water-limited (red) and energy-limited (blue) by DI. Note that neither energy nor water availability explained GPP_T_{opt} well when the dryness index was between 0.77 and 1.06 (Fig. S3) and it is difficult to define whether these sites are water-limited or energy-limited. Thus sites with dryness index between 0.77 and 1.06 were excluded from the analysis to avoid confusion (Fig. S3). We end up with 33 sites and 385 site-year data for energy-limited sites, 27 site and 252 site-year data for water-limited sites.

All statistical analyses were performed using R x64 3.3.1 for Windows at α level=0.05. Graphs were constructed using package "ggplot2".

3. Results and discussions

3.1. Nonlinear control of climate variables over GPP_T_{opt}

Soil moisture (SM), global solar radiation (GSR), mean annual temperature (MAT) and air vapor pressure deficit (VPD) explained 47% of the spatial variation in GPP_T_{opt} (Fig. 2, Table S1). Our ridge regression analysis suggested that mean annual precipitation (MAP), growing season precipitation (GSP) and dryness index (DI) are lurking variables for GPP_T_{opt} (Table S1). Soil moisture was the most important climate variable for controlling GPP_T_{opt}, explaining 36% of the spatial variation by itself (Figs. 2a and S4, Table S2). GPP_T_{opt} linearly increased with soil moisture but plateaued when soil moisture is larger than 353 ± 39 mm and maintained a constant GPP_T_{opt} at the rate of 8 g C m^{-2} d^{-1} (Fig. 2a). GPP_T_{opt}-precipitation function showed a similar non-linear saturation pattern and the saturation points for growing season precipitation and mean annual precipitation were 306 ± 39 and 804 ± 55 mm, respectively (Table S2). Similar relationship is observed between aboveground net primary productivity and precipitation across large spatial scales (Luo et al., 2017).

Temperature and global solar radiation (GSR) represent thermal and light energy respectively. Vapor pressure deficit (VPD) is a combined effect of thermal energy and water. GPP_T_{opt}-energy response curves were nonlinear concave down across space. The turning points of GSR, MAT, and VPD were 13.5 MJ m^{-2} d^{-1}, 8.5 °C and 0.8 kPa, respectively (Fig. 2b–d, Table S2). These turning points of energy delineate a low-energy range over which GPP_T_{opt} increased with increasing energy and a high-energy range over which GPP_T_{opt} decreased with excess energy. V$_{cmax}$ is modeled to linearly increase with light, which explains overestimated photosynthetic capacity in wet, tropical forest since a linear function fails to capture the suppression of photosynthetic capacity at high light level (Smith et al., 2019). During the periods of global dimming, plants photosynthesized more efficiently and sequestrated more carbon (Wild, 2009), agreeing with our results since most sites locate in a radiation range that further increase in GSR suppresses GPP_T_{opt} (Fig. 2b).

3.2. The effects of climate variables depend on the dryness condition

The existence of the thresholds of soil moisture indicates a transition from water-controlled stage to energy-controlled stage for GPP_T_{opt}. Therefore, the effects of soil moisture, light, temperature and air dryness depended on dryness conditions, as indicated by the significant interaction between these climate variables and DI (Table 1). We divided sites into energy-limited group and water-limited group (Fig. 3) based on the balance between water demand (PET, potential evapotranspiration) and water supply (P, precipitation), using the same concept of Budyko's curve (Budyko, 1961; Budyko et al., 1974) that well-describes evapotranspiration.

The response function of GPP_T_{opt} to soil moisture, air temperature and vapor pressure deficit became linear within water- and energy-limited group (Table 2). Thus, we were able to extract the partial linear slope of GPP_T_{opt} to soil moisture, air dryness and mean annual temperature along the dryness gradients using moving window analysis. Variations caused by solar radiation were represented by a third-degree polynomial function since GPP_T_{opt}-GSR response curve is still nonlinear within water-limited and energy-limited groups (Table 2).

GPP_T_{opt} linearly increased with soil moisture ($P = 0.002$, Table 2) and became increasingly more sensitive to soil moisture along the dryness gradients (Fig. 3a). However, the sensitivity to water peaked when dryness index was around 2.1–2.4 and decreased with further increase in aridity. Vegetation types that occur in extremely arid region have relatively low productivity and highly adapted mechanisms to cope with extreme drought compared with semiarid regions, causing the reduced sensitivity of GPP_T_{opt} to soil moisture when dryness index was larger than 2.4 (Liu et al., 2018, 2020). GPP_T_{opt} linearly increased with soil
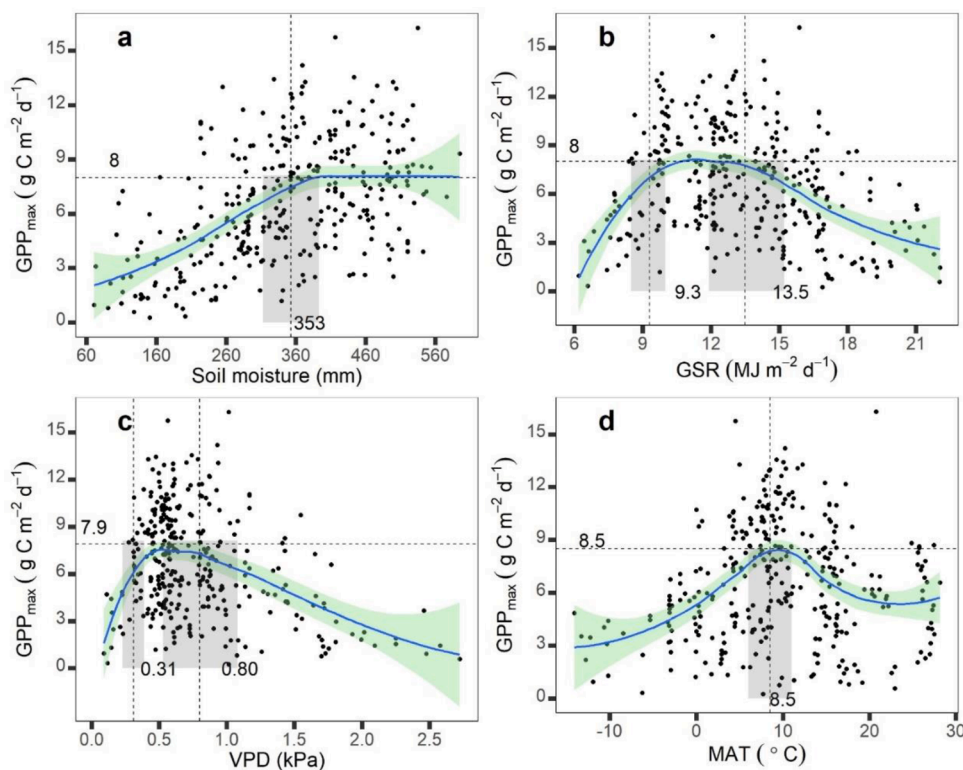
Fig. 2. Effects of soil moisture, global solar radiation (GSR), vapor pressure deficit (VPD) and mean annual temperature (MAT) on GPP_T_{opt}. GPP_T_{opt} (g C m^{-2} d^{-1}) is plotted against soil moisture (SM, mm), global solar radiation (GSR, MJ m^{-2} d^{-1}), vapor pressure deficit (VPD, kPa) and mean annual temperature (MAT, °C). The blue line is the weighted least squares fit determined by a nearest neighbor algorithm (LOESS) and light green shadow represents the 95% confidence interval. The vertical dashed line indicates the turning points of each climate variables and the grey shadow is the 95% confidence interval calculated by segmented regression. The horizontal dashed line indicates the peak GPP_T_{opt} at optimum climate conditions.

Table 1

Analysis of variance of the interaction between climate variables and dryness index. Climate variables: Soil moisture (SM, mm), Global solar radiation (GSR, MJ m^{-2} d^{-1}), Growing season vapor pressure deficit (VPD, kPa), Dryness index (DI, PET/P), Mean annual temperature (MAT, °C), Growing season precipitation (GSP, mm yr^{-1}), Growing season temperature (GST, °C), Mean annual precipitation (MAP, mm yr^{-1}). GPP_T_{opt} is log transformed.

	Sum Sq	Mean Sq	F value	P	
SM	41.43	41.43	167.17	<0.001	**
VPD	5.75	5.75	23.2	<0.001	**
MAT	3.37	3.37	13.58	<0.001	**
GSR	2.29	2.29	9.23	0.003	*
DI	0	0	0.01	0.913	N.S
SM*DI	2.09	2.09	8.42	0.004	*
VPD*DI	0.98	0.98	3.95	0.048	*
MAT*DI	5.44	5.44	21.93	<0.001	**
GSR*DI	2.31	2.31	9.31	0.002	*

moisture across water-limited sites and did not affect GPP_T_{opt} across energy-limited sites (Table 2, Fig. 3a). Consequently, a nonlinear saturation function was observed between GPP_T_{opt} and soil moisture across the 326 sites, supporting the double asymmetric model of the controlling of water availability over carbon cycles (Knapp et al., 2017). The linear increase in GPP_T_{opt} with soil moisture across water-limited sites is consistent with the linear increment of carbon process with water availability in grassland that often occurs in water-limited habitat (Zhou et al., 2009). V_{cmax} model excludes the influence of soil moisture or precipitation (Smith et al., 2019) because its parameters are derived from greenhouse studies that did not consider the influences from drought. Thus, the current model might overestimate GPP_T_{opt} in water-limited regions. Since soil moisture is the most important climate variable for controlling GPP_T_{opt} (Fig. S4), it is imperative to include soil moisture into the model for estimating GPP_T_{opt}.

High air temperature enhanced GPP_T_{opt} ($P = 0.012$, Table S1, Fig. 3b), similar to the leaf model that V_{cmax} increases with air temperature (Smith et al., 2019). Warming-induced air dryness enhanced

GPP_T_{opt} in very mesic regions but suppressed GPP_T_{opt} in dry regions (Fig. 3c). Air dryness consistently reduced GPP_T_{opt} across sites with a dryness index larger than 1.5 (Fig. 3c), which is also defined as dryland by UNESCO (Unesco, 1979). Ecosystem carbon process is generally depressed in water-logged environment (Taylor et al., 2017), explaining air dryness caused stimulation of GPP_T_{opt} in mesic areas. GPP_T_{opt} is withheld by air dryness in water-limited regions, consistent with a recent study reporting that increased air dryness reduces the global vegetation growth in the new era (Yuan et al., 2019). High temperature induced increase in vapor pressure deficit is also accused for faster mortality of tree seedlings common to the forest–grassland ecotone (Will et al., 2013). However, the leaf-level model assumes an increase of V_{cmax} with VPD throughout the whole range of VPD (Smith et al., 2019). Leaf-level knowledge about photosynthetic capacity is from greenhouse studies that usually do not impose drought stress, which possibly explains the discrepancy between leaf-level and ecosystem-level knowledge. Thus, only the most mesic sites benefit from increasing VPD (Fig. 3c). Direct upscaling of leaf-level knowledge to ecosystem level will overestimate the carbon uptake capacity in water-limited regions.

GPP_T_{opt} is determined by and increases with water or energy, depending on which one is more limiting. The strong climate control of GPP_T_{opt} (R^2: 40%–50%, Fig. S3) supports photosynthetic coordination theory that photosynthetic capacities are controlled by climate, instead of soil nitrogen (Prentice et al., 2013; Smith et al., 2019). However, neither energy nor water availability explained GPP_T_{opt} well when water-limit and energy-limit reached equilibrium (dryness index between 0.77 and 1.06, Fig. S3). The decoupling of climate variables and GPP_T_{opt} was reflected by the oscillation of the slopes when dryness index was around 1 (Fig. 2). Other factors, such as soil nutrients and microbes, possibly come into play when energy-limit and water-limit reach equilibrium.

None of the previous study has ever revealed that the major climate variable for GPP_T_{opt} differs between water-limited and energy-limited sites. Therefore, ignoring the effects of dryness causes bias because the estimated parameters would depend on the ratio of water-limited sites to energy-limited sites. In addition, a model generated for the whole globe
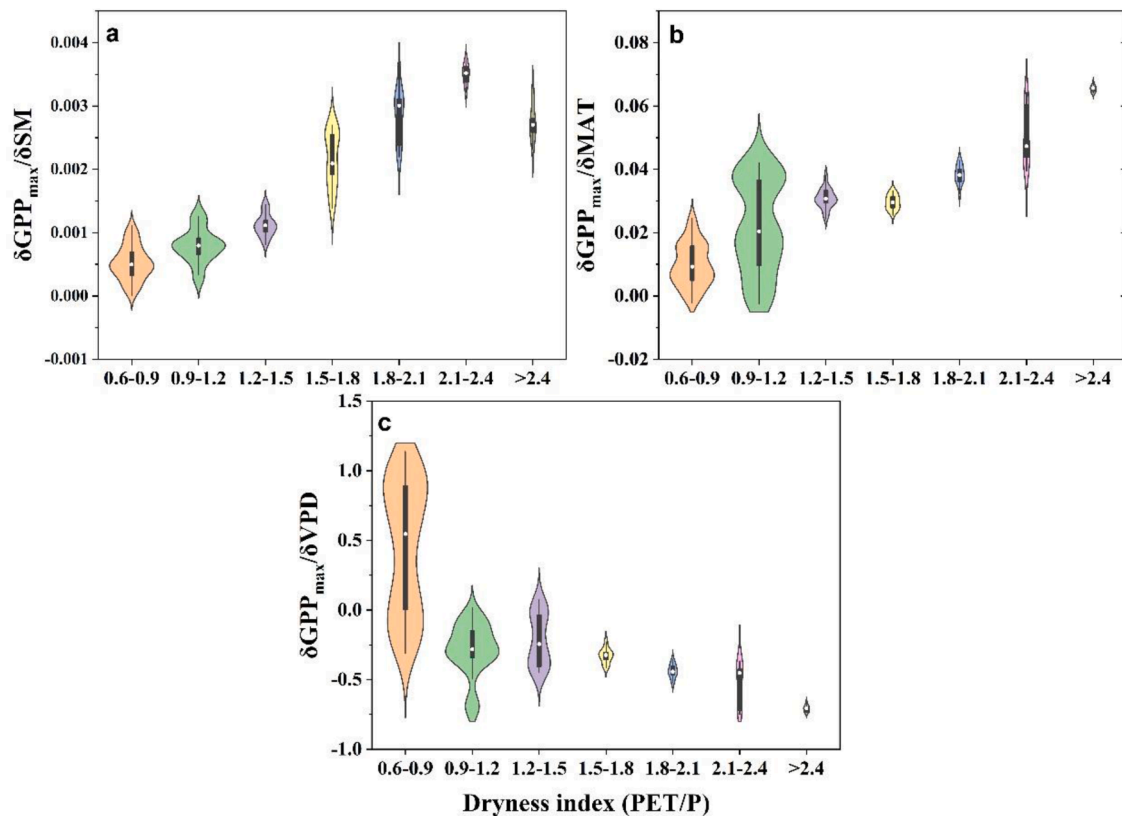
Fig. 3. Dependence of the sensitivity of GPP_T_{opt} to climate variables on the dryness gradients. Violin plots of the sensitivity of GPP_T_{opt} to soil moisture (SM) (a), mean annual temperature (MAT) (b), and vapor pressure deficit (VPD) (c) across the dryness gradients (PET/P). White dots indicate the median values, black boxes cover the interquartile range, and thin black lines reach the 5th and 95th percentiles.

may work well in mesic region but not in drylands, or vice versa. Grouping sites based on the most limiting factor and applying different algorithms more realistically represents the nature process, as a result, improving the accuracy of ESMs' projection of carbon influx in the future.

3.3. Temporal variation in GPP_T_{opt} as influenced by water- and energy-limitation

Dryness affects the temporal variation in GPP_T_{opt} in response to mean annual temperature (MAT) and mean annual precipitation (MAP). Inter-annual change in MAT does not affect the temporal variation in GPP_T_{opt} in energy-limited sites yet reduces GPP_T_{opt} by 0.17 g C m^{-2} d^{-1} per 1 °C increase in MAT ($P = 0.01$, Fig. 4a, c). GPP_T_{opt} tends to be higher in wetter years in both energy- and water-limited sites (Fig. 4b, d). However, water-limited sites are about 1.6 times more sensitive to changes in precipitation than energy-limited sites. Consequently, drought causes greater reduction in carbon uptake in water-limited regions. Given the relationship between carbon uptake and GPP_T_{opt}, energy-limited sites are more likely to maintain a stable carbon uptake across years while water-limited sites are more susceptible to warming or drought. This rationale is in agreement with a recent report that water-limited regions are responsible for most of the inter-annual variation (IAV) in atmospheric CO_2 growth rate. The predicted wide-spreading drought by the next century (Girvetz and Zganjar, 2014) will turn many energy-limited ecosystems into water-limited ecosystems, indicating a larger IAV of atmospheric CO_2 growth rate in the future.

3.4. The response of GPP_T_{opt} to climate variables also depends on vegetation types

Incorporating vegetation types increased R^2 from 47% to 67% (Tables S2 and S3), substantially improving the prediction power of the model. The sensitivity of GPP_T_{opt} to MAT and soil moisture varied among vegetation types (Fig. 5). Warming tended to increase GPP_T_{opt} in vegetation types that inhabit wetter climate. Vegetation types that inhabit drier climate, such as grassland, are more responsive to changes in soil moisture. We normalized GPP_T_{opt} by excluding the influence of climate variables. The normalized GPP_T_{opt} still varied among vegetation types ($P < 0.001$, Table S3), probably due to evolutionary adaptation to local environment (Huang et al., 2018). Shrub and Savanna, which inhabited the most arid niche, showed the lowest GPP_T_{opt} even with climate variables adjust to the same value (Fig. 5c). Our finding indicates that when a natural ecosystem degraded to a less productive vegetation type, carbon sequestration is suppressed even if climate conditions go back to the previous conditions. Genetic selection or human management such as irrigation and fertilization possibly explains the higher normalized GPP_T_{opt} in cropland (Fig. 5c), agreeing with previous studies that expanding cropland increase in maximum NDVI over time (Huang et al., 2018) and the land-use management in China and India lead the greening of earth (Chen et al., 2019).

3.5. Global distribution of GPP_T_{opt}

We predicted current global distribution of GPP_T_{opt} based on temperature, light, soil moisture, air dryness and vegetation types (Fig. S5). The global average GPP_T_{opt} is 3.6 g C m^{-2} d^{-1}, with spatial variations that echo the global distribution of GPP perfectly (Beer et al., 2010). Highest GPP_T_{opt} occurs along the equator, followed by humid and temperate regions such as the great lake area in the U.S, southeast China

Table 2

Influences of climate variables in energy-limited (DI < 1) versus water-limited (DI > 1) regions. Soil moisture (SM, mm), Global solar radiation (GSR, MJ m^{-2} d^{-1}), Growing season vapor pressure deficit (VPD, kPa), Dryness index (DI, PET/P), Mean annual temperature (MAT, °C), Growing season precipitation (GSP, mm yr^{-1}), Growing season temperature (GST, °C), Mean annual precipitation (MAP, mm yr^{-1}). GPP_T$_{opt}$ is log transformed. Coefficients that are significant at α=0.05 level are bolded.

Group		Slope	SE	t-value	P		R^2	AIC
Energy-limited	SM[1]	0.55	0.61	0.90	0.368	N.S	0.28	194
DI < 1	SM[2]	-0.43	0.56	-0.77	0.442	N.S		
n = 143	GSR[1]	-0.54	0.85	-0.64	0.521	N.S		
	GSR[2]	**-1.55**	**0.58**	**-2.67**	**0.008**	*		
	GSR[3]	**1.90**	**0.52**	**3.67**	**<0.001**	**		
	GST	0.01	0.02	0.26	0.80	N.S		
	MAT	0.01	0.01	0.66	0.51	N.S		
	VPD	0.37	0.33	1.11	0.27	N.S		
Water-limited	**SM[1]**	**2.10**	**0.68**	**3.11**	**0.002**	*	0.53	268
DI > 1	SM[2]	-0.84	0.53	-1.57	0.118	N.S		
n = 183	**GSR[1]**	**-4.45**	**0.98**	**-4.52**	**<0.001**	**		
	GSR[2]	**-1.91**	**0.59**	**-3.24**	**0.001**	*		
	GSR[3]	0.97	0.55	1.77	0.078	N.S		
	GST	0.01	0.02	0.36	0.718	N.S		
	MAT	**0.04**	**0.01**	**3.35**	**0.001**	**		
	VPD	**-0.51**	**0.16**	**-3.22**	**0.002**	*		

and Europe (Fig. 6). Water deficiencies constrained GPP_T$_{opt}$ (Fig. 6) and GPP (Beer et al., 2010) in subtropical region, disagreeing with the leaf-level model that predicts a high V_{cmax} in the same region (Smith et al., 2019). The discrepancies between ecosystem and leaf knowledge contribute to different projections of carbon uptake capacity. The lack of constraining from water contributes to overestimated V_{cmax} in water-limited regions (Smith et al., 2019). We also found GPP_T$_{opt}$ to be negative related with VPD in water-limited regions while modelled V_{cmax} continuously increases with VPD throughout the whole range (Smith et al., 2019). Furthermore, GPP_T$_{opt}$-radiation response curve is non-linear concave down while V_{cmax} is modeled to linearly increase with irradiance (Smith et al., 2019). A better representation of the nonlinear relationship between carbon uptake processes and light helps to reduce the uncertainty in the prediction of carbon fluxes (Nicole and Gordon, 2017).

4. Conclusions

We found a strong regulation of the maximum gross primary productivity (GPP_T$_{opt}$) across space by soil moisture, light, temperature, air dryness and vegetation types. Responses of GPP_T$_{opt}$ to climate variables depend on dryness gradients. GPP_T$_{opt}$ is limited by temperature under wet condition while GPP_T$_{opt}$ is limited by water availability under dry condition. The concept of water and energy limits, which originates from researches concerning evapotranspiration, applies to the spatiotemporal variation in GPP_T$_{opt}$. Global warming only reduces carbon uptake capacity of water-limited sites due to warming-aggravated water deficiencies and air dryness. Energy-limited ecosystems are able to maintain its carbon uptake capacity or even benefit from warming. The responses of GPP_T$_{opt}$ to climate variables also depend on vegetation types. GPP_T$_{opt}$ tends to be higher in vegetation types with humid climates and is more likely to benefit from a warmer climate without water deficit stress. These knowledge does not only improve our understanding of the photosynthetic processes at the ecosystem level, but also aid the modelers to improve the accuracy of coupled climate-carbon cycle process model.

Data accessibility statement

All FLUXNET data can be downloaded at: https://fluxnet.fluxdata.org. Climate variables of each site were obtained from WorldClim (https://www.worldclim.org/). Humidity index was obtained from FAO dataset (https://www.fao.org/home/en/). Soil moisture is obtained from CPC soil moisture data provided by the NOAA/OAR/ESRL PSD, Boulder, Colorado, USA, from their Web site at https://www.esrl.noaa.
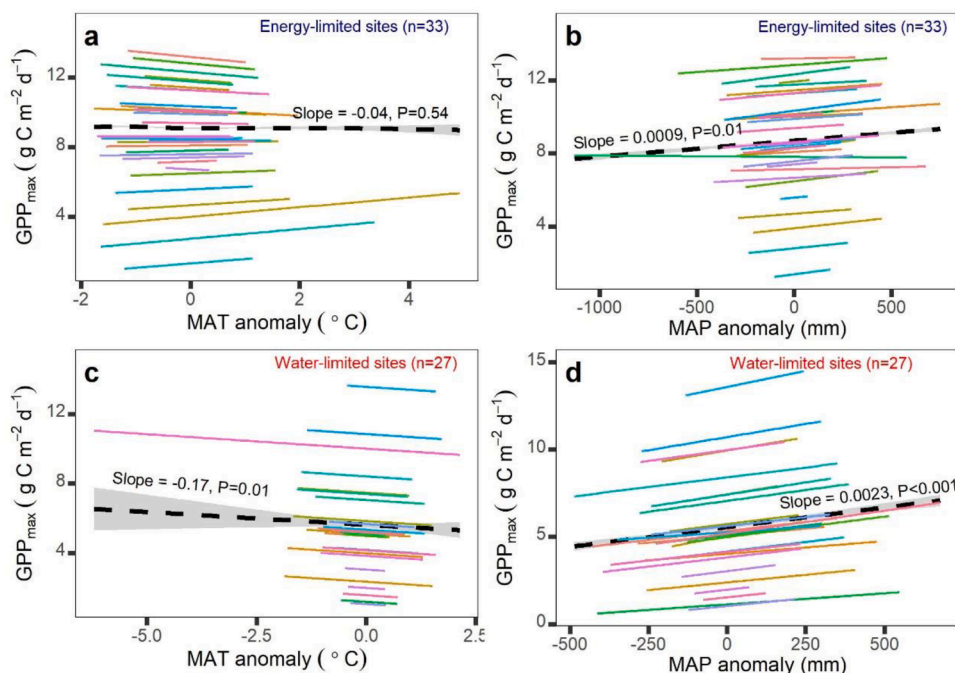
Fig. 4. Relationship of temporal variation in GPP_T$_{opt}$ with mean annual temperature (MAT, °C) and mean annual precipitation (MAP, mm) depends on dryness. Mean annual temperature and precipitation's effects on the temporal variation in GPP_T$_{opt}$ in 33 energy-limited sites (a, b). Mean annual temperature and precipitation's effects on the temporal variation in GPP_T$_{opt}$ in 27 water-limited sites (c, d). There are 385 site-year and 252 site-year data for energy-limited and water-limited sites, respectively. Black dashed lines are the fixed effect linear regression slope between sites from the mixed-effect model; colored lines indicate the temporal patterns within sites. Climate anomaly is calculated by deducing the mean value of each site from the value of each year of that site.
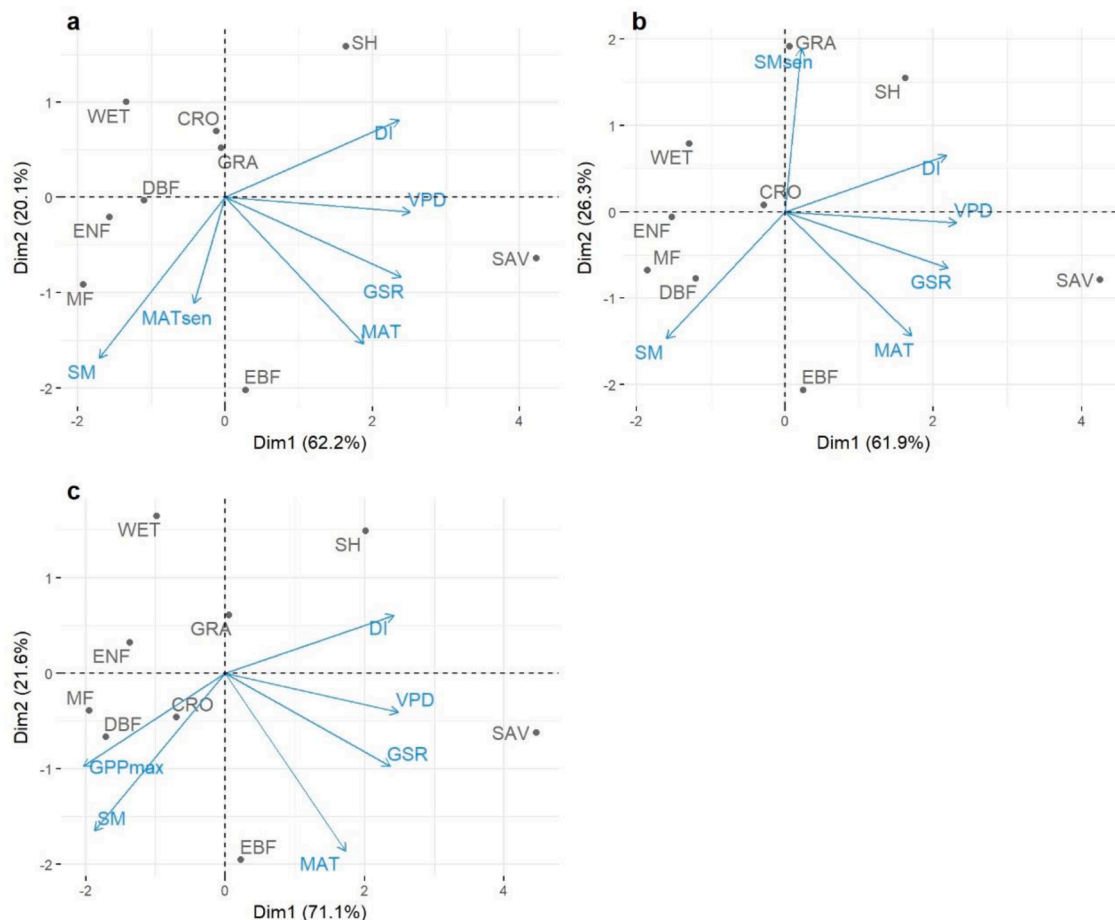
Fig. 5. Climatic preference of habitat among vegetation types in relation to the spatial sensitivity of GPP_T_{opt}. The sensitivity of GPP_T_{opt} to mean annual temperature (MAT$_{sen}$) in relation to the climatic preferences of vegetation types (a). The sensitivity of GPP_T_{opt} to soil moisture (SM$_{sen}$) among vegetation types in relation to the climatic preferences of vegetation types (b). Normalized GPP_T_{opt} in relation to the climatic preferences of vegetation types (c). Principle component analysis (PCA) is used to investigate the relationship between climatic preference of vegetation types and MAT$_{sen}$, SM$_{sen}$, and normalized GPP_T_{opt}. Normalized GPP_T_{opt} is calculated by adjust MAT, GSR, SM and VPD to the mean level of the dataset (see material and method). The angle of two arrows indicates the relationship of the two variables.
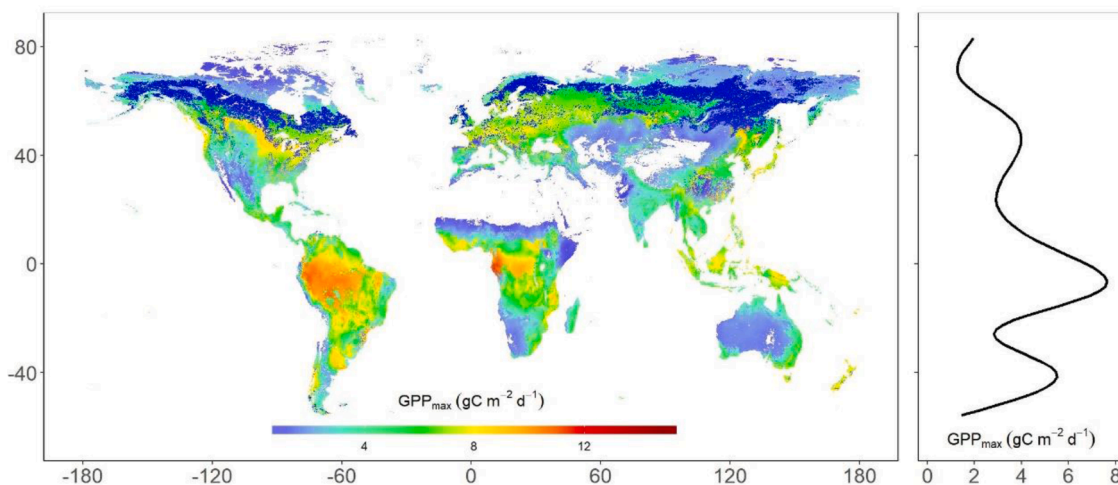
Fig. 6. Globally predicted present GPP_T_{opt}. GPP_T_{opt} is computed using global solar radiation, mean annual temperature, growing season precipitation, soil moisture and vegetation types as predictors with resolution of 0.1°×0.1°. GPP_T_{opt} is regressed on latitude using generalized additive model (GAM), as shown in the right panel.

gov/psd/.

Declaration of Competing Interest

The authors declare that they have no known competing financial interests or personal relationships that could have appeared to influence the work reported in this paper.

Acknowledgments

Supplementary materials

Supplementary material associated with this article can be found, in the online version, at doi:10.1016/j.agrformet.2022.109073.

References

Beer, C., Ciais, P., Reichstein, M., Baldocchi, D., Law, B.E., Papale, D., Soussana, J.F., Ammann, C., Buchmann, N., Frank, D., Gianelle, D., Janssens, I.A., Knohl, A., Köstner, B., Moors, E., Roupsard, O., Verbeeck, H., Vesala, T., Williams, C.A., Wohlfahrt, G., 2009. Temporal and among-site variability of inherent water use efficiency at the ecosystem level. Glob. Biogeochem. Cycles 23, GB2018.

Beer, C., Reichstein, M., Tomelleri, E., Ciais, P., Jung, M., Carvalhais, N., Rödenbeck, C., Arain, M.A., Baldocchi, D., Bonan, G.B., Bondeau, A., Cescatti, A., Lasslop, G., Lindroth, A., Lomas, M., Luyssaert, S., Margolis, H., Oleson, K.W., Roupsard, O., Veenendaal, E., Viovy, N., Williams, C., Woodward, F.I., Papale, D., 2010. Terrestrial gross carbon dioxide uptake: global distribution and covariation with climate. Science 329, 834.

Budyko, M.I., 1961. The heat balance of the earth's surface. Sov. Geogr. 2, 3–13.

Budyko, M.I., Miller, D.H., Miller, D.H., 1974. Climate and Life. Academic press, New York.

Chen, C., Park, T., Wang, X., Piao, S., Xu, B., Chaturvedi, R.K., Fuchs, R., Brovkin, V., Ciais, P., Fensholt, R., Tømmervik, H., Bala, G., Zhu, Z., Nemani, R.R., Myneni, R.B., 2019. China and India lead in greening of the world through land-use management. Nat. Sustain. 2, 122–129.

H. Chu, D.D. Baldocchi, R. John, S. Wolf, M. Reichstein (2017) Fluxes all of the time? A primer on the temporal representativeness of FLUXNET. J. Geophys. Res. Biogeosci. 122, 289–307.

Fick, S.E., Hijmans, R.J., 2017. WorldClim 2: new 1-km spatial resolution climate surfaces for global land areas. Int. J. Climatol. 37, 4302–4315.

Food and Agriculture Organization of the United Nations, 2015. FAO Geonetwork. FAO, Rome, Italy.

Friedlingstein, P., O'Sullivan, M., Jones, M.W., Andrew, R.M., Hauck, J., Olsen, A., Peters, G.P., Peters, W., Pongratz, J., Sitch, S., Le Quéré, C., Canadell, J.G., Ciais, P., Jackson, R.B., Alin, S., Aragão, L.E.O.C., Arneth, A., Arora, V., Bates, N.R., Becker, M., Benoit-Cattin, A., Bittig, H.C., Bopp, L., Bultan, S., Chandra, N., Chevallier, F., Chini, L.P., Evans, W., Florentie, L., Forster, P.M., Gasser, T., Gehlen, M., Gilfillan, D., Gkritzalis, T., Gregor, L., Gruber, N., Harris, I., Hartung, K., Haverd, V., Houghton, R.A., Ilyina, T., Jain, A.K., Joetzjer, E., Kadono, K., Kato, E., Kitidis, V., Korsbakken, J.I., Landschützer, P., Lefèvre, N., Lenton, A., Lienert, S., Liu, Z., Lombardozzi, D., Marland, G., Metzl, N., Munro, D.R., Nabel, J.E.M.S., Nakaoka, S.I., Niwa, Y., O'Brien, K., Ono, T., Palmer, P.I., Pierrot, D., Poulter, B., Resplandy, L., Robertson, E., Rödenbeck, C., Schwinger, J., Séférian, R., Skjelvan, I., Smith, A.J.P., Sutton, A.J., Tanhua, T., Tans, P.P., Tian, H., Tilbrook, B., van der Werf, G., Vuichard, N., Walker, A.P., Wanninkhof, R., Watson, A.J., Willis, D.,

Wiltshire, A.J., Yuan, W., Yue, X., Zaehle, S., 2020. Global carbon Budget 2020. Earth Syst. Sci. Data 12, 3269–3340.

Girvetz, E.H., Zganjar, C., 2014. Dissecting indices of aridity for assessing the impacts of global climate change. Clim. Chang. 126, 469–483.

Gu, L., Post, W.M., Baldocchi, D.D., Black, T.A., Suyker, A.E., Verma, S.B., Vesala, T., Wofsy, S.C., 2009. Characterizing the seasonal dynamics of plant community photosynthesis across a range of vegetation types. Phenology of Ecosystem Processes. Springer, Dordrecht/New York.

Huang, K., Xia, J., Wang, Y., Ahlström, A., Chen, J., Cook, R.B., Cui, E., Fang, Y., Fisher, J.B., Huntzinger, D.N., Li, Z., Michalak, A.M., Qiao, Y., Schaefer, K., Schwalm, C., Wang, J., Wei, Y., Xu, X., Yan, L., Bian, C., Luo, Y., 2018. Enhanced peak growth of global vegetation and its key mechanisms. Nat. Ecol. Evol. 2, 1897–1905.

Huang, M., Piao, S., Ciais, P., Peñuelas, J., Wang, X., Keenan, T.F., Peng, S., Berry, J.A., Wang, K., Mao, J., Alkama, R., Cescatti, A., Cuntz, M., De Deurwaerder, H., Gao, M., He, Y., Liu, Y., Luo, Y., Myneni, R.B., Niu, S., Shi, X., Yuan, W., Verbeeck, H., Wang, T., Wu, J., Janssens, I.A., 2019. Air temperature optima of vegetation productivity across global biomes. Nat. Ecol. Evol. 3, 772–779.

Humphrey, V., Zscheischler, J., Ciais, P., Gudmundsson, L., Sitch, S., Seneviratne, S.I., 2018. Sensitivity of atmospheric CO_2 growth rate to observed changes in terrestrial water storage. Nature 560, 628–631.

Huxman, T.E., Smith, M.D., Fay, P.A., Knapp, A.K., Shaw, M.R., Loik, M.E., Smith, S.D., Tissue, D.T., Zak, J.C., Weltzin, J.F., Pockman, W.T., Sala, O.E., Haddad, B.M., Harte, J., Koch, G.W., Schwinning, S., Small, E.E., Williams, D.G., 2004. Convergence across biomes to a common rain-use efficiency. Nature 429, 651.

Knapp, A.K., Ciais, P., Smith, M.D., 2017. Reconciling inconsistencies in precipitation–productivity relationships: implications for climate change. New Phytol. 214, 41–47.

Kumarathunge, D.P., Medlyn, B.E., Drake, J.E., Tjoelker, M.G., Aspinwall, M.J., Battaglia, M., Cano, F.J., Carter, K.R., Cavaleri, M.A., Cernusak, L.A., Chambers, J. Q., Crous, K.Y., De Kauwe, M.G., Dillaway, D.N., Dreyer, E., Ellsworth, D.S., Ghannoum, O., Han, Q., Hikosaka, K., Jensen, A.M., Kelly, J.W.G., Kruger, E.L., Mercado, L.M., Onoda, Y., Reich, P.B., Rogers, A., Slot, M., Smith, N.G., Tarvainen, L., Tissue, D.T., Togashi, H.F., Tribuzy, E.S., Uddling, J., Vårhammar, A., Wallin, G., Warren, J.M., Way, D.A., 2019. Acclimation and adaptation components of the temperature dependence of plant photosynthesis at the global scale. New Phytol. 222, 768–784.

Lin, Y.S., Medlyn, B.E., Duursma, R.A., Prentice, I.C., Wang, H., Baig, S., Eamus, D., Dios, V.R.D., Mitchell, P., Ellsworth, D.S., 2015. Optimal stomatal behaviour around the world. Nat. Clim. Chang. 5, 459–464.

Liu, L., Gudmundsson, L., Hauser, M., Qin, D., Li, S., Seneviratne, S.I., 2020. Soil moisture dominates dryness stress on ecosystem production globally. Nat. Commun. 11, 4892.

Liu, L., Peng, S., AghaKouchak, A., Huang, Y., Li, Y., Qin, D., Xie, A., Li, S., 2018. Broad consistency between satellite and vegetation model estimates of net primary productivity across global and regional scales. J. Geophys. Res. Biogeosci. 123, 3603–3616.

Luo, Y., Jiang, L., Niu, S., Zhou, X., 2017. Nonlinear responses of land ecosystems to variation in precipitation. New Phytol. 214, 5–7.

Musavi, T., Migliavacca, M., Reichstein, M., Kattge, J., Wirth, C., Black, T.A., Janssens, I., Knohl, A., Loustau, D., Roupsard, O., Varlagin, A., Rambal, S., Cescatti, A., Gianelle, D., Kondo, H., Tamrakar, R., Mahecha, M.D., 2017. Stand age and species richness dampen interannual variation of ecosystem-level photosynthetic capacity. Nat. Ecol. Evol. 1, 0048.

Nicole, S.L., Gordon, B.B., 2017. Reducing uncertainty in projections of terrestrial carbon uptake. Environ. Res. Lett. 12, 044020.

Niu, S., Luo, Y., Fei, S., Yuan, W., Schimel, D.S., Ammann, C., Arain, M.A., Arneth, A., Aubinet, M., Barr, A., 2012. Thermal optimality of net ecosystem exchange of carbon dioxide and underlying mechanisms. New Phytol. 194, 775–783.

Peel, M., Finlayson, B., McMahon, T., 2007. Updated world map of the Koppen-Geiger climate classification. Hydrol. Earth Syst. Sci. 11, 1633–1644.

Potter, N.J., Zhang, L., 2009. Interannual variability of catchment water balance in Australia. J. Hydrol. 369, 120–129.

Prentice, I., Dong, N., Gleason, S., Maire, V., Wright, I., 2013. Balancing the costs of carbon gain and water transport: testing a new theoretical framework for plant functional ecology. Ecol. Lett. 17, 82–91.

Reich, P.B., Sendall, K.M., Stefanski, A., Rich, R.L., Hobbie, S.E., Montgomery, R.A., 2018. Effects of climate warming on photosynthesis in boreal tree species depend on soil moisture. Nature 562, 263–267.

Sendall, K.M., Reich, P.B., Zhao, C., Jihua, H., Wei, X.O., Stefanski, A., Rice, K., Rich, R. L., Montgomery, R.A., 2015. Acclimation of photosynthetic temperature optima of temperate and boreal tree species in response to experimental forest warming. Glob. Chang. Biol. 21, 1342–1357.

Smith, N.G., Dukes, J.S., 2018. Drivers of leaf carbon exchange capacity across biomes at the continental scale. Ecology 1610–1620.

Smith, N.G., Keenan, T.F., Colin Prentice, I., Wang, H., Wright, I.J., Niinemets, Ü., Crous, K.Y., Domingues, T.F., Guerrieri, R., Yoko Ishida, F., 2019. Global photosynthetic capacity is optimized to the environment. Ecol. Lett. 22, 506–517.

Taylor, P.G., Cleveland, C.C., Wieder, W.R., Sullivan, B.W., Doughty, C.E., Dobrowski, S. Z., Townsend, A.R., 2017. Temperature and rainfall interact to control carbon cycling in tropical forests. Ecol. Lett. 20, 779–788.

Unesco, 1979. Map of the World Distribution of Arid Regions: Explanatory Note. UNESCO.

Wang, H., Prentice, I.C., Keenan, T.F., Davis, T.W., Wright, I.J., Cornwell, W.K., Evans, B. J., Peng, C., 2017. Towards a universal model for carbon dioxide uptake by plants. Nat. Plants 3, 734–741.

Way, D.A., Yamori, W., 2014. Thermal acclimation of photosynthesis: on the importance of adjusting our definitions and accounting for thermal acclimation of respiration. Photosynth. Res. 119, 89–100.

Whittaker, R., 1975. Communities and Ecosystems, 2nd ed. Macmillan Publishing Company.

Wild, M., 2009. Global dimming and brightening: a review. J. Geophys. Res. Atmos. 114, 31.

Will, R.E., Wilson, S.M., Zou, C.B., Hennessey, T.C., 2013. Increased vapor pressure deficit due to higher temperature leads to greater transpiration and faster mortality during drought for tree seedlings common to the forest–grassland ecotone. New Phytol. 200, 366–374.

Xia, J., Niu, S., Ciais, P., Janssens, I.A., Chen, J., Ammann, C., Arain, A., Blanken, P.D., Cescatti, A., Bonal, D., Buchmann, N., Curtis, P.S., Chen, S., Dong, J., Flanagan, L.B., Frankenberg, C., Georgiadis, T., Gough, C.M., Hui, D., Kiely, G., Li, J., Lund, M., Magliulo, V., Marcolla, B., Merbold, L., Montagnani, L., Moors, E.J., Olesen, J.E., Piao, S., Raschi, A., Roupsard, O., Suyker, A.E., Urbaniak, M., Vaccari, F.P., Varlagin, A., Vesala, T., Wilkinson, M., Weng, E., Wohlfahrt, G., Yan, L., Luo, Y., 2015. Joint control of terrestrial gross primary productivity by plant phenology and physiology. Proc. Natl. Acad. Sci. U. S. A. 112, 2788–2793.

Yi, C., Jackson, N., 2021. A review of measuring ecosystem resilience to disturbance. Environ. Res. Lett. 16, 053008.

Yi, C., Rustic, G., Xu, X., Wang, J., Dookie, A., Wei, S., Hendrey, G., Ricciuto, D., Meyers, T., Nagy, Z., Pinter, K., 2012. Climate extremes and grassland potential productivity. Environ. Res. Lett. 7, 035703.

Yu, G., Song, X., Wang, Q., Liu, Y., Guan, D., Yan, J., Sun, X., Zhang, L., Wen, X., 2008. Water-use efficiency of forest ecosystems in eastern China and its relations to climatic variables. New Phytol. 177, 927–937.

Yuan, W., Zheng, Y., Piao, S., Ciais, P., Lombardozzi, D., Wang, Y., Ryu, Y., Chen, G., Dong, W., Hu, Z., Jain, A.K., Jiang, C., Kato, E., Li, S., Lienert, S., Liu, S., Nabel, J.E. M.S., Qin, Z., Quine, T., Sitch, S., Smith, W.K., Wang, F., Wu, C., Xiao, Z., Yang, S., 2019. Increased atmospheric vapor pressure deficit reduces global vegetation growth. Sci. Adv. 5, eaax1396.

Zhou, S., Zhang, Y., Caylor, K.K., Luo, Y., Xiao, X., Ciais, P., Huang, Y., Wang, G., 2016. Explaining inter-annual variability of gross primary productivity from plant phenology and physiology. Agric. For. Meteorol. 226-227, 246–256.

Zhou, X., Talley, M., Luo, Y., 2009. Biomass, litter, and soil respiration along a precipitation gradient in southern great plains, USA. Ecosystems 12, 1369–1380.